Acta Geotechnica (2021) 16:1909–1921
https://doi.org/10.1007/s11440-020-01109-1

RESEARCH PAPER

Centrifuge study on behavior of rigid pile composite foundation under embankment in soft soil

Jian-lin Yu[1,2] · Jia-jin Zhou[1,2] · Xiao-nan Gong[1,2] · Ri-qing Xu[1,2] · Jun-yuan Li[3] · Shan-dai Xu[1,2]

Received: 25 December 2019 / Accepted: 6 November 2020 / Published online: 25 November 2020

Abstract

The rigid pile composite foundation is widely used in highway projects in soft soil area as it can effectively increase the bearing capacity and stability of the foundation. While the research on the behavior and failure mode of rigid pile composite foundation under embankment is not enough, instability failure of rigid pile composite foundation often occurs in practical projects. This paper presents a centrifuge model test to investigate the load transfer mechanism, settlement characteristic and failure mode of rigid pile composite foundation under embankment. The test results show that: the soil displacement of different region in rigid pile composite foundation was different, obvious vertical displacement occurred in the soil under the center of embankment and the horizontal displacement was very small in this region; both vertical and horizontal displacement occurred in the soil under the shoulder of embankment; and obvious horizontal displacement occurred in the soil under the slope toe of embankment; moreover, ground heave also occurred near the slope toe of embankment. The soil displacement in rigid pile composite foundation had a large influence on the stress characteristic and failure mode of rigid piles, the compressive failure and bending failure would probably occur for the piles under the center and shoulder of the embankment, respectively, and the tension-bending failure would probably occur for the piles under the slope toe of embankment. The different failure modes of piles at different regions should be considered in the design of rigid pile composite foundation under embankment. The test results can be used to improve the design method for rigid pile composite foundation under embankment in practical projects.

Keywords Centrifuge model test · Embankment · Failure mode · Rigid pile composite foundation · Soft soil

1 Introduction

The rigid pile composite foundation is widely used in expressway and high-speed railway projects because of its high bearing capacity, little post-construction settlement and rapid construction speed [7, 19, 31]. The behavior of composite foundation under embankment has been investigated by many researchers through theoretical methods [1, 6, 9, 13, 26, 27, 29, 33, 41, 45] and numerical methods [11, 16, 17, 20, 30, 40, 42, 43]. Moreover, field tests [3, 4, 32, 38, 39, 44], model tests [15, 36, 37] and centrifuge model tests [1, 2, 8, 24, 47] were also used to investigate the behavior of composite foundation under embankment. Nevertheless, in the previous researches, the composite foundation under embankment was mostly taken as a semi-infinite space, and a typical element was adopted to investigate the pile-soil stress ratio and settlement characteristic caused by the soil arching effect.

With the rapid development of urban construction in China, the height of embankment becomes higher and higher and instability failure often occurs in the rigid pile composite foundation under embankment, as shown in Fig. 1.

How to correctly evaluate the stability of rigid pile composite foundation under embankment has become a critical issue in road construction projects. The conventional limit equilibrium analysis method for composite

✉ Jia-jin Zhou
zhoujiajin@zju.edu.cn

[1] Research Center of Coastal and Urban Geotechnical Engineering, Zhejiang University, Hangzhou 310058, China

[2] Zhejiang Urban Underground Space Development Engineering Research Center, Zhejiang University, Hangzhou 310058, China

[3] Taizhou Transportation Bureau, Taizhou 318000, China

Fig. 1 Photographs of instability failure of rigid pile composite foundation under embankment

foundation under embankment assumed that a sliding surface occurred owing to the shear failure of pile shaft [18, 35], as shown in Fig. 2. The numerical analysis results showed that the assumption of shear failure of pile shaft

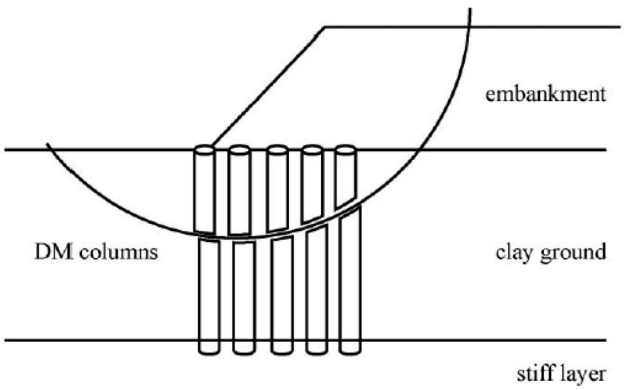

Fig. 2 Sketch of limit equilibrium method (from Kitazume and Maruyama 2007 [23])

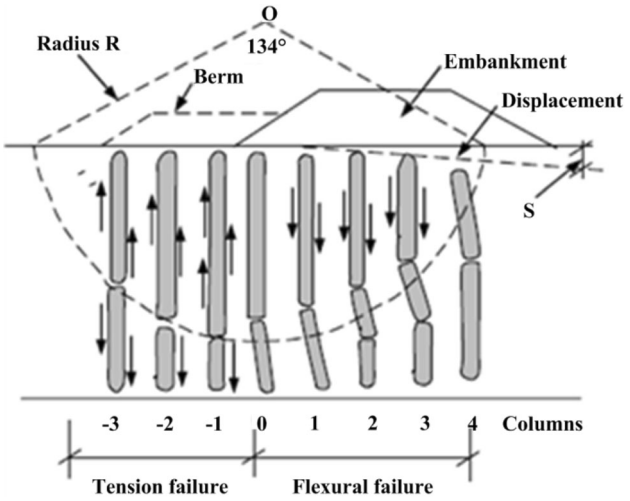

Fig. 3 Possible failure modes of cement mixing piles (from Broms 2003 [5])

overestimated the stability of embankment over cement mixing pile [11, 14, 30]. Zheng et al. [46] proposed a damage plasticity model to study the progressive failure of rigid piles under an embankment load, and the simulation results showed that the essential failure mode for rigid piles was tensile failure, which was primarily governed by the distribution of the bending moment and the axial force within the piles. The centrifuge model test results showed that the failure mode of cement mixing pile was not only dependent on the external loading, but also affected by the location of piles. The piles at different regions had different failure modes, like shear failure, bending failure, tension failure, pile shaft inclination or lateral movement failure [12, 21–23, 28, 34].

Broms [5] also pointed out that the cement mixing piles at different regions had two failure modes: bending failure and tension failure, as shown in Fig. 3. Nevertheless, the research on the stability analysis of rigid pile composite foundation under embankment is rather little, and the study on the stress characteristics and failure modes of the piles at different regions is also not enough. The instability failure of rigid pile composite foundation under embankment often occurs in practical projects. More researches are needed to give a deeper investigation on the stability analysis of rigid pile composite foundation under embankment.

In this paper, the behavior of rigid pile composite foundation under embankment was investigated through a centrifuge model test. The variable acceleration load method, constant acceleration load method and gasbag load method were adopted to simulate the embankment filling stage, post-construction service stage and progressive failure stage, respectively. The settlement characteristic and load transfer mechanism of composite foundation, pile-

Fig. 4 Photograph of ZJU-400 geotechnical centrifuge

soil stress ratio and the variation of excess pore water pressure in the test process were analyzed based on the tests results.

2 Centrifuge model test

In the centrifuge model test, the centrifuge can create a stress field which is identical to the stress field of full-scale test, and the load transfer mechanism and settlement characteristic of full-scale test can be simulated through model scale test. The centrifuge model test was conducted in the ZJU-400 geotechnical centrifuge, as shown in Fig. 4. The effective rotation radius of the centrifuge was 4.5 m, and the effective volume of the container was 1.5 m × 1.2 m × 1.5 m. The capacity of the centrifuge was 400 g t, with a maximum centrifuge acceleration of 150 g.

2.1 Foundation soil preparation

According to the similarity theory of centrifuge model test, the stress of model foundation in centrifuge will be increased to n·g when the centrifuge acceleration is n·g. The model scale of the centrifuge test in this research was 100. In the centrifuge test, the coarse sand was used to simulate the gravel in the embankment, and the average particle size of the coarse sand was 0.5 mm. The relative density of the coarse sand was 70%. The Malaysia kaolin clay and Fujian sand were adopted as the soft soil layer and bearing layer, respectively. The specific gravity of the Fujian sand grain was 2.643, the mean particle size D_{50} was 0.17 mm, and the maximum and minimum void ratios were 0.952 and 0.607, respectively. The physical properties of Malaysia kaolin clay are presented in Table 1.

In the foundation preparation process, a layer of polytetrafluoroethylene (PTFE) was painted on the inner wall of the test chamber, to reduce the friction between the soil and inner wall of the test chamber. A permeable geotextile layer was set at the bottom of the test chamber to act as the drainage boundary. The air pluviation method was used to make the base sand layer. The height of the sand layer was 100 mm, and the relative density was 60%. The vacuum mixing method was used to stir the kaolin clay. The kaolin clay layer was filled above the sand layer, and the thickness of kaolin clay layer was 180 mm.

The test chamber was moved into the centrifuge after the kaolin clay was rested in the chamber for 48 h, and the initial consolidation of clay layer took 6 h under a centrifuge acceleration of 100 g. After initial consolidation, the test chamber was moved out from the centrifuge and a 5.5-cm-thick sand layer was filled above the kaolin clay layer. The test chamber was then moved into the centrifuge again for surcharge consolidation. The centrifuge acceleration was increased to 100 g, and the settlement of foundation soil surface tended to be stable after 3 h. The consolidation of clay layer could be considered to be completed at this time. The T-bar test was then adopted to measure the undrained shear strength of the clay layer, and the variation of undrained shear strength of clay along the depth is presented in Fig. 5. This figure shows that the undrained shear strength of clay increased from 0 to 9 kPa when the soil layer depth increased from 0 to 0.8 m. The undrained shear strength then increased almost linearly with the soil layer depth, and the undrained shear strength reached 41 kPa at the base of clay layer. The undrained shear strength (s_u) was commonly related the vertical effective stress (σ'_{v0}) and over-consolidation ratio (OCR) of the soil layer [10]:

$$\left(\frac{s_u}{\sigma'_{v0}}\right)_{OC} = \left(\frac{s_u}{\sigma'_{v0}}\right)_{NC} \cdot \left[\frac{\sigma'_{vm}}{\sigma'_{v0}}\right]^m = a \cdot OCR^m, \quad (1)$$

Table 1 Physical properties of Malaysia kaolin clay

G_s	γ (kN/m^3)	w (%)	PL (%)	LL (%)	e	k (cm/s)	C_v (m^2/year)
2.64	16.0	45.5	36.5	60.7	1.2	2.0×10^{-8}	40

G_s is specific gravity; γ is unit weight; w is water content; PL and LL are plastic limit and liquid limit, respectively; e is void ratio; k is coefficient of permeability; and C_v is coefficient of consolidation

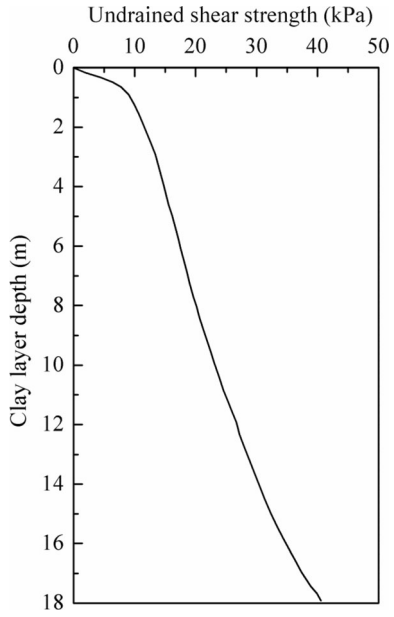

Fig. 5 Variation of undrained shear strength of clay layer along the depth

in which σ'_{vm} is the pre-consolidated stress, a and m are two constants. The constant a refers to the strength ratio for a normally consolidated profile, and the constant m represents the increasing rate of strength ratio with OCR.

In this research, the kaolin clay layer could be approximately considered as normally consolidated soil, and the value of a was about 0.14. The value of constant a in this research was close to the reported ranges $0.17 < a < 0.24$ for natural clays [10].

2.2 Model pile

The model piles were made by aluminum pipes. The density of aluminum pipe was 2.69 g/cm^3, and the elastic modulus and Poisson's ratio were 68.9 GPa and 0.33, respectively. The parameters of model pile and prototype concrete pile are presented in Table 2. The diameter of the model pile was 10 mm with a wall thickness of 0.4 mm, and pile length was 200 mm. The diameter of prototype concrete pile was 1000 mm with a wall thickness of 120 mm, and the pile length was 20 m. The bending stiffness and compressive stiffness of the model pile were both close to that of prototype concrete pile under 100 g centrifuge acceleration condition.

An aluminum block was equipped at the pile head to act as the pile cap. The side length of prototype pile cap was 2 m, and the height was 0.5 m. The elastic modulus of the concrete of pile cap was 28 GPa, and the bending stiffness of prototype pile cap was about 5.8×10^8 N m^2. The side length and height of the aluminum block were 20 mm and 3.7 mm, respectively, to guarantee that the bending stiffness of the model pile cap was similar to the bending stiffness of the prototype pile cap. A tapered aluminum block was set at the pile tip, and the angle of the tapered block was 60°. A layer of plastic net was covered on the model pile head to simulate the geogrid on pile head. The tensile strength of plastic net was 1.738 kN/m, and the tensile strength of geogrid was 160 kN/m.

In the centrifuge model test, three model piles were equipped with strain gauges to measure the axial force, and another three model piles were equipped with strain gauges to measure the bending moment of the pile shaft. The model pile and the layout of the strain gauges are presented in Fig. 6. Figure 6b shows that five groups of strain gauges were equipped along the pile shaft, and the location of strain gauges of six test piles was the same. The first group of strain gauges was equipped 20 mm away from the pile head, and the distance of the neighboring stain gauges was 40 mm. The six test piles were all calibrated before the centrifuge test.

2.3 Layout of test piles and transducers

The layout of the test piles and transducers is presented in Fig. 7. It can be seen in Fig. 7a that the height of the embankment was 60 mm, and the slope grade was 1:1.5. According to the symmetry of the model test, one half of the embankment model was built in the centrifuge test. The width of the embankment surface was 200 mm. Figure 7a also shows that three pore water pressure transducers were buried 5 cm under the ground surface, and the pore water pressure transducers P1, P2 and P3 were buried under the shoulder, center and slope toe of the embankment, respectively. Two laser displacement transducers D1 and

Table 2 Summary of model and prototype pile parameters

Pile type	Diameter (mm)	Wall thickness (mm)	Length (m)	Elastic modulus (GPa)	Bending stiffness (N m^2)	Compressive stiffness (N)
Prototype pile	1000	120	20	30	9.81×10^8	10.0×10^9
Model pile	10	0.4	0.2	68.9	9.59	8.3×10^5

(a) Photograph of model pile

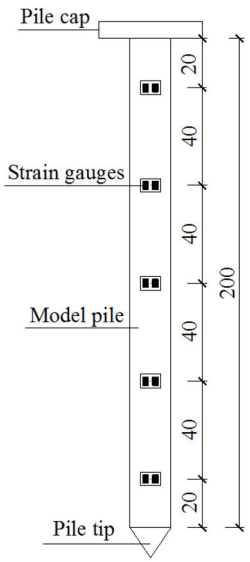

(b) Layout of strain gauges (unit: mm)

Fig. 6 Schematic of model pile

D2 were used to measure the displacement of the soil near the slope toe of embankment. Moreover, the particle image velocimetry (PIV) method was adopted to measure the soil displacement in the test process.

Figure 7b shows that the axial force of model piles Z1–Z3 and the bending moment of model piles W1–W3 were measured in the test process. The model piles Z1–Z3 were located at the same side of the symmetry axis of the model foundation soil, and model piles W1–W3 were placed at the other side of the model foundation soil. Moreover, four micro-soil pressure transducers (T1–T4) were adopted to measure the pressures of pile head and the soil between the piles, respectively. The micro-soil pressure transducer T1 and T4 were buried in the soil between the piles, and T2 and T3 were buried on the pile head.

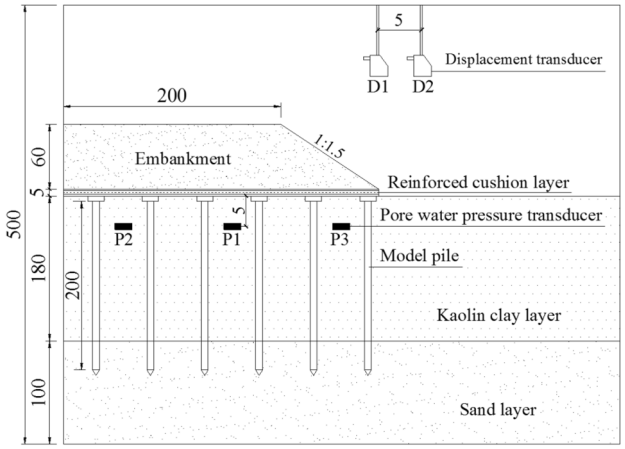

(a) Elevation view

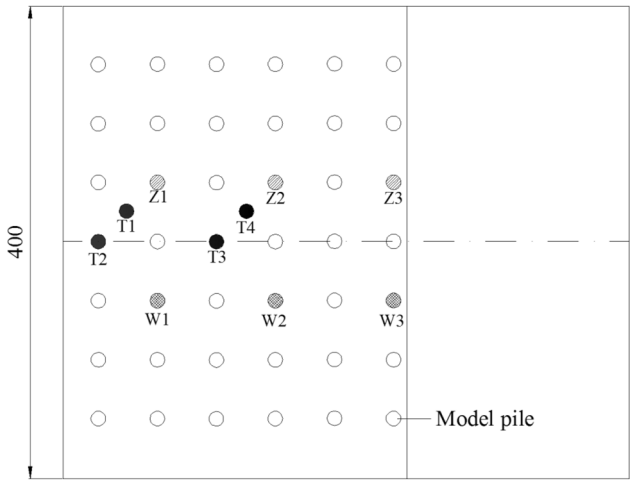

(b) Plan view

Fig. 7 Layout of model piles and transducers (unit: mm)

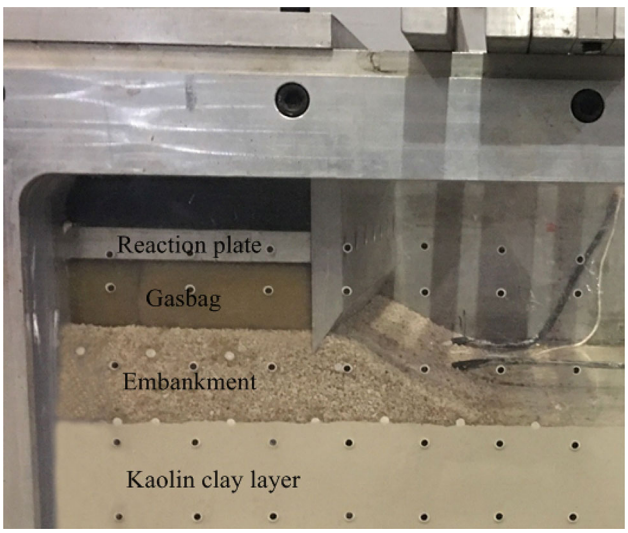

Fig. 8 Gasbag loading device

2.4 Gasbag loading device

To simulate the progressive failure process of embankment, an inflatable rubber gasbag was adopted to apply pressure on the surface of embankment in the loading process. This loading method could eliminate the influence of the stiffness of loading plate on the behavior of embankment, and the applied pressure on the surface of embankment could keep homogeneous even after the settlement occurred at embankment surface. The gasbag should keep inflated in the loading process, and a reaction plate was set at the back side of the gasbag. The gasbag loading device contained a rubber gasbag, a reaction plate and an automatic inflating device, as shown in Fig. 8.

2.5 Test procedure

Assume that the embankment was filled by three layers, and the height of one filling layer was 2 m for prototype embankment. The centrifuge acceleration of each filling step could be calculated according to the assumption that the stress in the centrifuge test was identical to that in the prototype embankment, as follows,

$$\frac{N\gamma S_{\mathrm{m}}}{L_{\mathrm{m}}} = \frac{\gamma S_{\mathrm{pi}}}{L_{\mathrm{p}}}, \tag{2}$$

in which S_{pi} is the cross-section area of prototype embankment after filling step i; S_{m} is the cross-section area of model embankment; γ is the unit weight of the soil; L_{m} the length of the bottom surface of model embankment and L_{p} is the length of the bottom surface of prototype embankment. The centrifuge acceleration of each filling step $N = S_{\mathrm{pi}}/100S_{\mathrm{m}}$, as $L_{\mathrm{p}} = 100L_{\mathrm{m}}$ in this research.

The centrifuge test was conducted after the foundation soil was filled in the test chamber and the transducers were equipped properly. The variable acceleration method was adopted to simulate the embankment filling process. The variation of centrifuge acceleration with time in the centrifuge test is presented in Fig. 9.

It can be seen in Fig. 9 that the centrifuge acceleration was firstly increased to 37.4 g in 5 min and kept constant for 7 min, and then it was increased to 70.8 g in 4.5 min and kept constant for 7.5 min; finally, the centrifuge acceleration was increased to 100 g in 4 min. After the embankment filling stage was completed, the centrifuge acceleration was kept at 100 g for another 100 min to simulate the working behavior of embankment in 700 days. After that, the gasbag was then used to apply pressure on

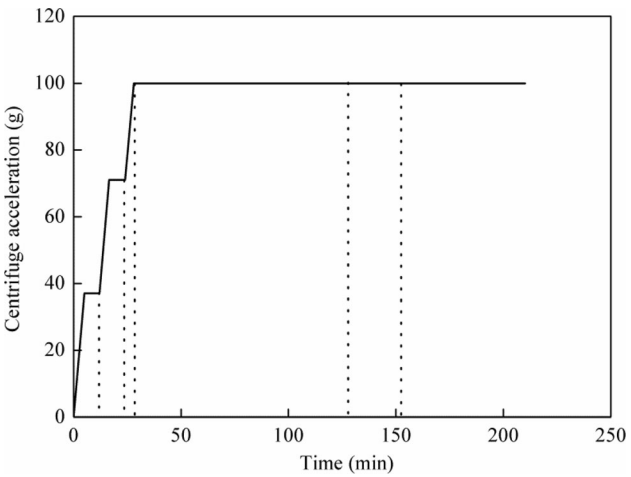

Fig. 9 Variation of centrifuge acceleration in centrifuge test

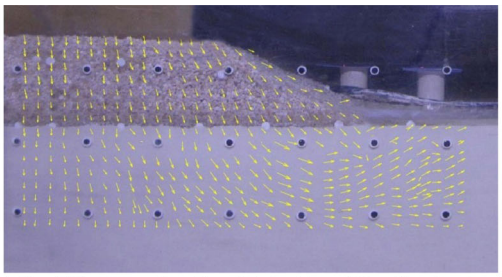

(a) Centrifuge acceleration 37.4g (Amplification factor 5)

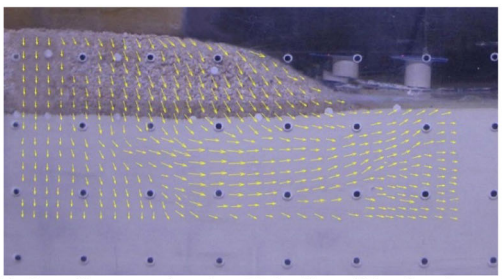

(b) Centrifuge acceleration 70.8g (Amplification factor 5)

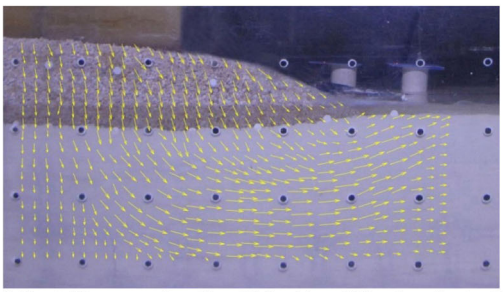

(c) Centrifuge acceleration 100g (Amplification factor 2)

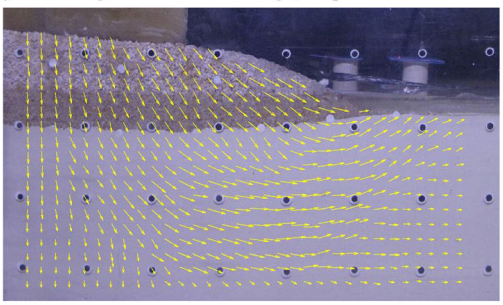

(d) Applied embankment surface pressure 200 kPa (Amplification factor 2)

Fig. 10 Soil displacement field at different stages in centrifuge test

the embankment surface to simulate the progressive failure process of embankment. The applied pressure was increased to the maximum value 200 kPa in 24 min, as the centrifuge acceleration was kept at 100 g.

3 Experimental results and analysis

3.1 Foundation soil displacement

The displacement field of foundation soil in centrifuge test can be obtained through PIV method. The displacement field of the model embankment and foundation soil at different stages are presented in Fig. 10. It can be seen in Fig. 10 that the displacement of foundation soil was gradually mobilized with the increase in centrifuge acceleration and applied embankment surface pressure. Moreover, the extent of area where horizontal displacement occurred also increased with the increase in centrifuge acceleration and applied embankment surface pressure. Figure 10 also shows that the displacement field of soil at different regions was different: obvious vertical displacement occurred in the soil under the center of embankment while the horizontal displacement was very small; both vertical and horizontal displacement occurred in the soil under the shoulder of embankment; and obvious horizontal displacement occurred in the soil under the slope toe of embankment; moreover, ground heave occurred near the slope toe of embankment. Figure 10d shows that an obvious circular sliding surface appeared in the foundation soil and instability failure tended to occur. Nevertheless, there was no horizontal displacement occurred in the soil under the center of embankment, which indicated that the instability failure of embankment tended to occur at the shoulder and slope toe of embankment.

3.2 Bending moment of pile shaft

The bending moment of the model test piles at different stages is presented in Fig. 11, in which N is the centrifuge acceleration and q is the applied embankment surface pressure. The test piles W1, W2 and W3 are under the center, shoulder and slope toe of the embankment, respectively, as shown in Fig. 7b. It can be seen in Fig. 11 that the bending moment of the test piles all increased with the increase in the centrifuge acceleration and applied embankment surface pressure. Figure 11a shows that the maximum bending moment of test pile W1 was 0.67 N m (at the depth of 10 cm). Figure 10b shows that the maximum bending moment of test pile W2 was 2.18 N m (at the depth of 14 cm), and the maximum bending moment of W2 was about 3.25 times the maximum bending moment of W1. The large bending moment in W2 was probably caused by the large horizontal displacement of the soil under the shoulder of the embankment, as shown in

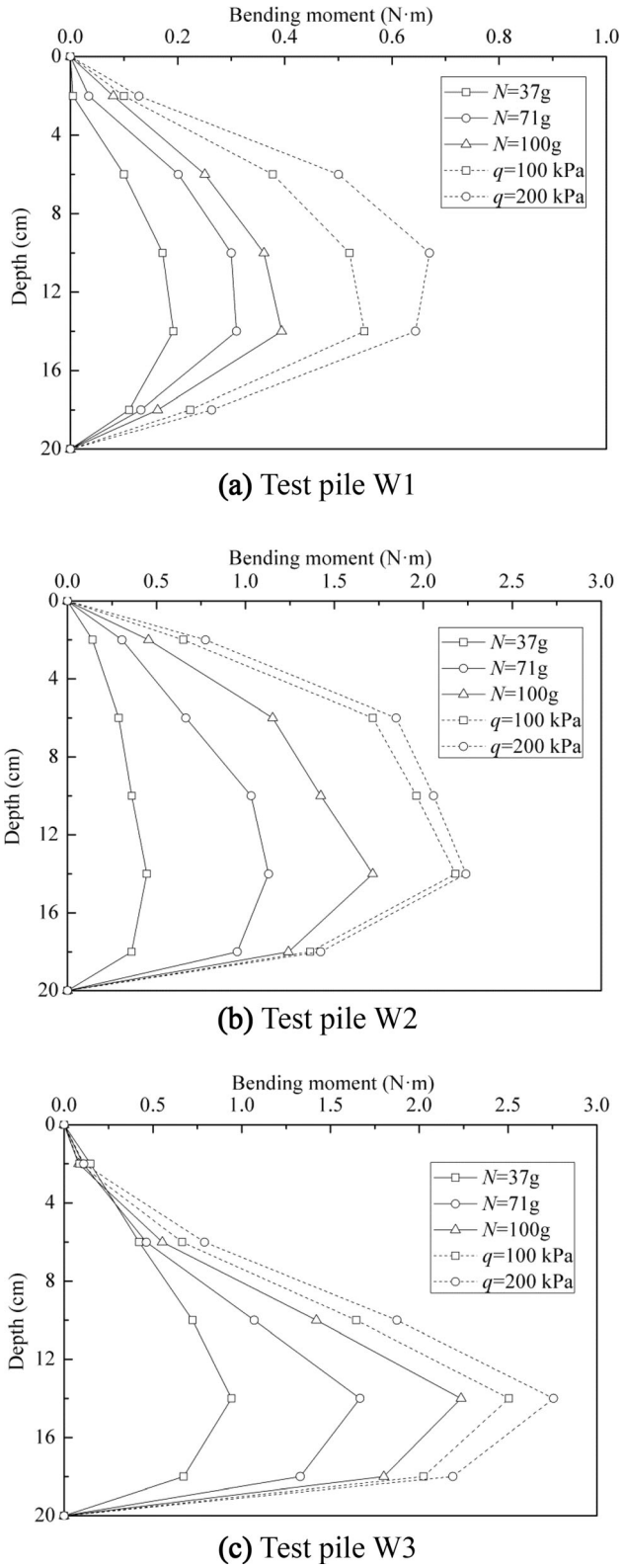

Fig. 11 Bending moment of test piles in centrifuge test

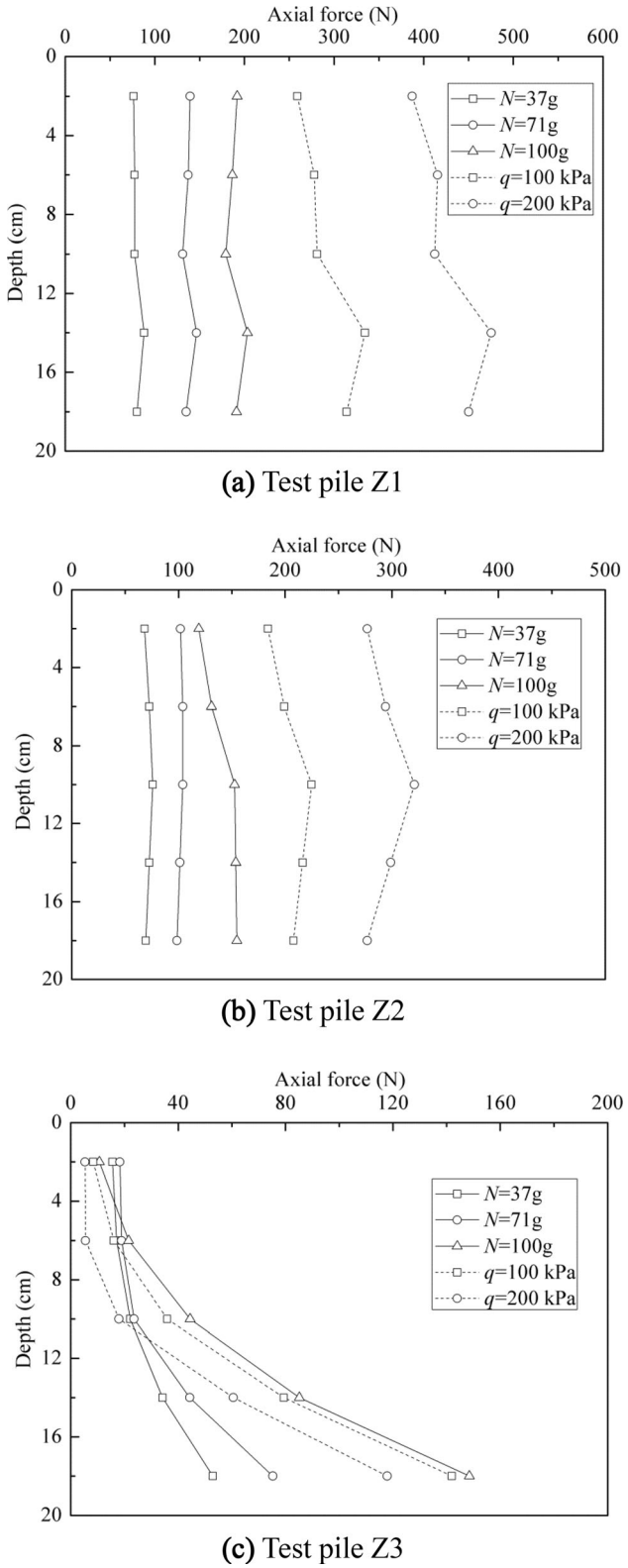

Fig. 12 Axial forces of test piles along pile shaft

Fig. 10. Figure 11c shows that W3 had the largest maximum bending moment 2.77 N m (at the depth of 14 cm). The largest maximum bending moment of W3 was consistent with the largest horizontal displacement of the soil under the slope toe of embankment, as shown in Fig. 10. It should be noted that the bending moment of W3 was very small at the depth of 0–6 cm, and this is probably because that ground heave occurred near the slope toe of embankment.

3.3 Axial force along pile shaft

The axial force of test piles Z1, Z2 and Z3 is presented in Fig. 12. The test piles Z1, Z2 and Z3 are under the center, shoulder and slope toe of the embankment, respectively. It can be seen in Fig. 12 that the test pile Z1 had the largest axial force, and the test pile Z3 had the smallest axial force among the three test piles.

It can also be seen in Fig. 12 that the axial force of Z1 and Z2 both increased with the increase in centrifuge acceleration and applied embankment surface pressure. The axial force of Z3 also increased with the increase in centrifuge acceleration, while the axial force of Z3 axial force decreased with the increase in applied embankment surface pressure. This is probably because that ground heave occurred near the slope toe of embankment, which induced uplift load on the pile shaft of Z3. It can also be noted from Fig. 12 that negative skin friction occurred at the upper part of test piles. This is because that the settlement of soil around the pile was larger than the settlement of the pile shaft. Moreover, the extent of negative skin friction at Z1 was larger than that at Z2, as the vertical displacement of soil around Z1 was larger than the vertical displacement of soil around Z2. Hence, for the composite foundation under flexible foundation like embankment, negative skin friction occurred at the upper part of pile shaft. The maximum axial force of pile was not at the pile head, which was different from the composite foundation under rigid foundation.

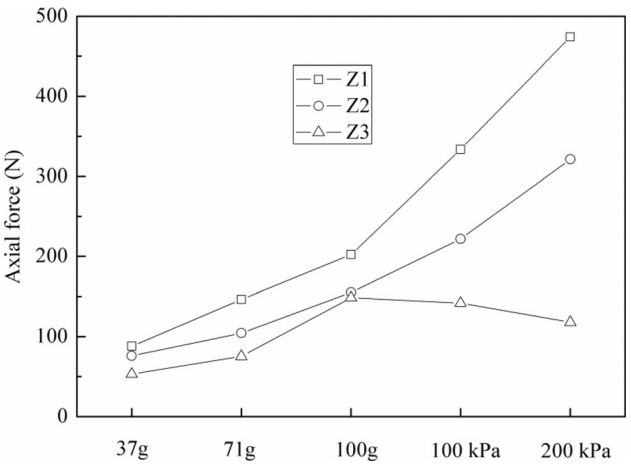

Fig. 13 Maximum axial forces of test piles Z1–Z3 at different stages

The variation of the maximum axial force of test piles Z1, Z2 and Z3 in the embankment filling and loading process is arranged as shown in Fig. 13. It can be seen in Fig. 13 that the axial forces of test piles all increased with the increase in centrifuge acceleration (the increase in embankment height), and the maximum axial forces of Z1, Z2 and Z3 were 201 kN, 158 kN and 136 kN, respectively, when the centrifuge acceleration reached 100 g. The axial force of pile under the center of embankment Z1 was larger than the axial forces of piles under shoulder and slope toe of embankment. It can also be seen in Fig. 13 that the axial forces of Z1 and Z2 both increased with the increase in applied embankment surface load, and the maximum axial forces of Z1 and Z2 were 479 kN and 323 kN, respectively, when the applied pressure increased to 200 kPa. The maximum axial force of Z1 was 1.48 times the maximum axial force of Z2, which indicated that the pile under the center of embankment was mainly to support the vertical load. Meanwhile, with the increase in applied pressure on the embankment surface, the ground heave occurred at the slope toe of embankment and the instability failure tended to occur. The axial force of test pile Z3 decreased because of the uplift load from the surrounding soil, and the maximum axial force of T3 decreased by 23% when the applied pressure increased from 0 kPa to 200 kPa. The maximum axial forces of Z1, Z2 and Z3 were 479 N, 323 N and 105 N, respectively, when the applied pressure reached 200 kPa, which indicated that the axial force of test piles at different regions was significantly different in rigid pile composite foundation under embankment.

3.4 Distribution of pore water pressure

The variation of pore water pressures in the test process is arranged as shown in Fig. 14. Unfortunately, the pore water pressure transducer P1 malfunctioned in the test process. The pore water pressure transducers P2 and P3 were equipped under the center and slope toe of embankment, respectively. The transducers P2 and P3 were both buried 5 cm under the ground surface, and the value of hydrostatic pressure for prototype foundation was 49 kPa. It can be seen in Fig. 14 that the excess pore water pressure under the center of embankment was larger than the excess pore water pressure under slope toe of embankment in the entire test process. The pore water pressures of P2 and P3 both increased with the increase in centrifuge acceleration, and the pore water pressures of P2 and P3 were 93 kPa and 79.5 kPa, respectively, when the centrifuge acceleration was increased to 100 g. The excess pore water pressure was then gradually dissipated as the centrifuge acceleration was kept at 100 g, and the pore water pressures of P2 and P3 decreased to 58.5 kPa and 51 kPa, respectively, after 700 days. The excess pore water pressures of P2 and P3

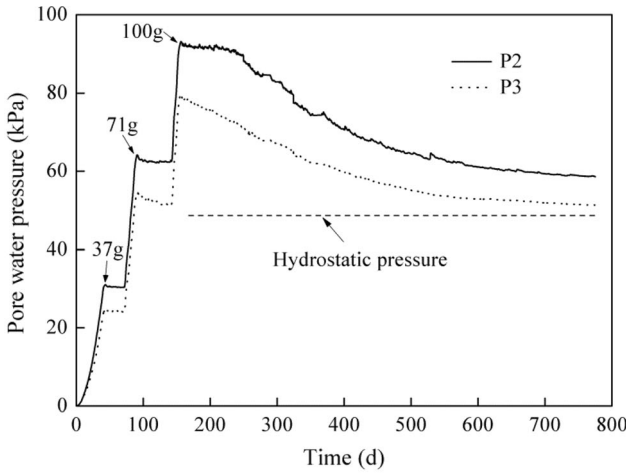

(a) Variation of pore water pressure with time in embankment filling process

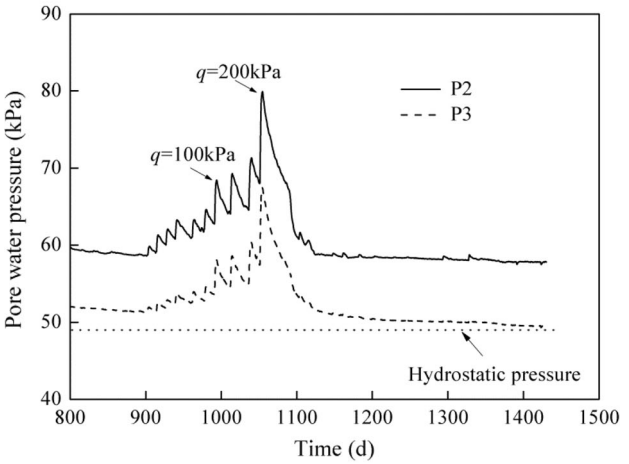

(b) Variation of pore water pressure with time in loading process

Fig. 14 Variation of pore water pressure with time in centrifuge test

were decreased by 78.4% and 93.4%, respectively, after 700 days, which indicated that the excess pore water pressure under slope toe of embankment dissipated faster than that under the center of embankment. Figure 14b shows that the pore water pressures of P2 and P3 both increased sharply when the pressure was applied on embankment surface. The excess pore water pressure was then gradually dissipated again with the time as the applied embankment surface pressure was kept at 200 kPa. Finally, the pore water pressures of P2 and P3 were decreased to 57.8 kPa and 49.3 kPa, respectively.

3.5 Pile-soil stress ratio

The variation of soil pressures and pile head pressures measured by soil pressure transducers T1–T4 is presented

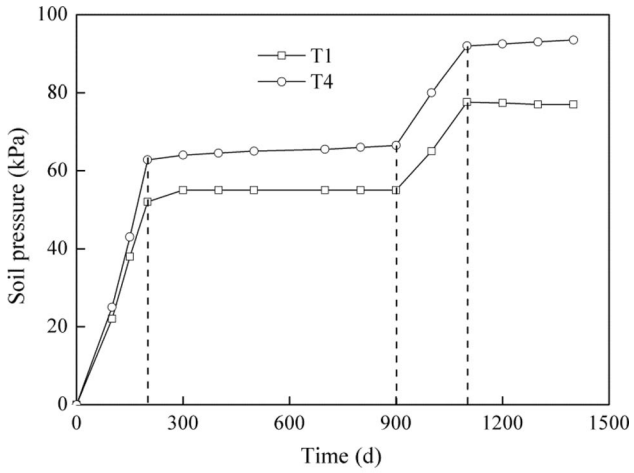

(a) Variation of soil stress with time

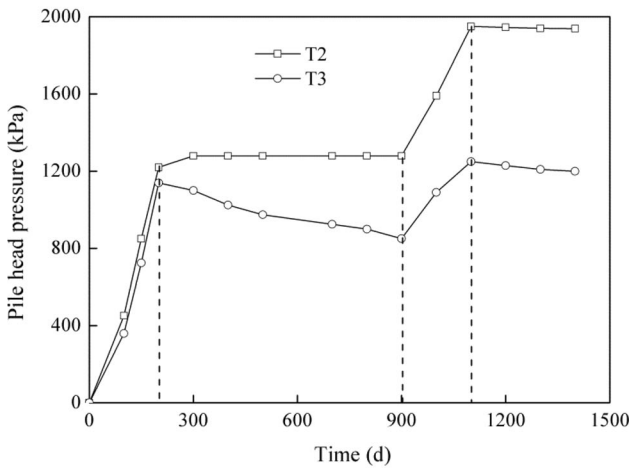

(b) Variation of pile head stress with time

Fig. 15 Variation of soil pressure and pile head pressure in the centrifuge test

in Fig. 15. The soil pressure transducers T1 and T4 were buried in the soil under the center and shoulder of the embankment, respectively. The transducers T2 and T3 were equipped on the head of test piles that were under the center and shoulder of the embankment, respectively. The centrifuge test could be divided into four stages: the embankment filling stage in the initial 200 days, post-construction service stage from 200 to 900 days, the loading stage from 900 to 1070 days and the final stage from 1070 to 1400 days. It can be seen from Fig. 15 that the soil pressures and pressures at pile head both increased with the increase in centrifuge acceleration and applied embankment surface pressure. The pile head pressures were much larger than the soil pressures, which indicated that the rigid pile in composite foundation supported the majority of load from the embankment. It can also be seen in Fig. 15 that the soil pressure under the center of embankment was smaller than the soil pressure under the shoulder of embankment, and the pile head pressure under the center of embankment was larger than the pile head pressure under the shoulder of embankment, which indicated that the pile under the center of embankment accounted for more vertical load compared to the pile under the center of embankment.

The variation of pile-soil stress ratios under the center and shoulder of embankment in the test process is presented in Fig. 16. This figure shows that the pile-soil stress ratio under the center of embankment increased with the increase in centrifuge acceleration in the embankment filling stage, and then the pile-soil stress ratio almost kept constant in the post-construction service stage. The pile-soil stress ratio under the shoulder of embankment also increased with the increase in centrifuge acceleration in the embankment filling stage, and the pile-soil stress ratio decreased slightly in the post-construction service stage. The variation of pile-soil stress ratio could be explained by the soil arching effect. The majority of embankment load would be transferred to the piles through the soil arching effect [25]. Hence, the pile-soil stress ratio increased in the embankment filling stage, and then almost kept constant in the post-construction service stage.

Figure 16 also shows that the maximum pile-soil stress ratio under the center and shoulder of the embankment in the loading process were 25.0 and 17.4, respectively. The pile-soil stress ratio under the center of embankment increased with the increase in applied embankment surface pressure, and the pile-soil stress ratio became constant when the applied embankment surface pressure was kept at 200 kPa. The pile-soil stress ratio under the shoulder of embankment decreased in the loading process, and the pile-soil stress ratio kept decreasing as the applied embankment surface pressure was kept at 200 kPa. The probable reason for the decrease in pile-soil stress ratio was that the bending

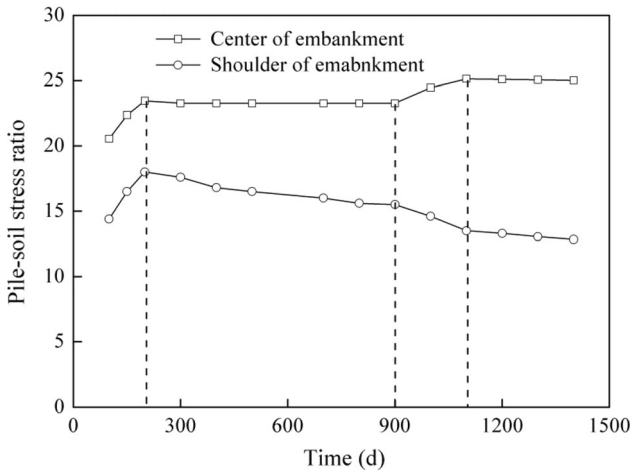

Fig. 16 Variation of pile-soil stress ratio at different stages

moment of pile increased because of the large horizontal displacement of the soil under the shoulder of embankment, and the instability failure of composite foundation tended to occur with the development of horizontal displacement of the soil.

4 Discussion

According to the analysis on the centrifuge test results, the distributions of axial force and bending moment of test piles at different regions were different. The pile location would affect the stress characteristics of pile shaft in composite foundation under embankment, and the displacement of soil between the piles also had a large effect on the stress characteristics of pile.

In the embankment filling and loading process, mainly vertical displacement occurred in soil under the center of embankment, and the rigid pile in this region was mainly under vertical load. Hence, the rigid pile under the center of embankment had the largest axial force and smallest bending moment. The compression failure would probably occur for the piles under the center of embankment. The "typical element" in a semi-infinite space which was commonly assumed in the conventional analytical method could only represent the behavior of composite foundation under the center of embankment.

In the loading process, both large vertical settlement and horizontal displacement occurred in the soil under the shoulder of the embankment. The bending moment of the pile shaft in this region increased with the increase in horizontal displacement of the soil. Moreover, the axial force of pile shaft also increased with the development of vertical displacement of soil. Considering that the compressive strength of rigid pile shaft was larger than its bending strength, the bending failure would probably occur for the piles under the shoulder of embankment.

With the increase in applied embankment surface pressure, large horizontal displacement and ground heave occurred at the slope toe of embankment, and the piles in this region were under lateral and uplift load. The bending moment of the pile increased in the loading process, while the axial force, especially the upper part of pile shaft, decreased with the increase in applied pressure. The tension-bending failure would probably occur for the piles in this region. The conclusions above were similar to the 3D finite element modeling results of rigid pile composite foundation under embankment [42, 43], as shown in Fig. 17.

It should be noted that the stress characteristics and failure modes of the rigid piles at different regions are different in rigid pile composite foundation under embankment. In the design of rigid pile composite

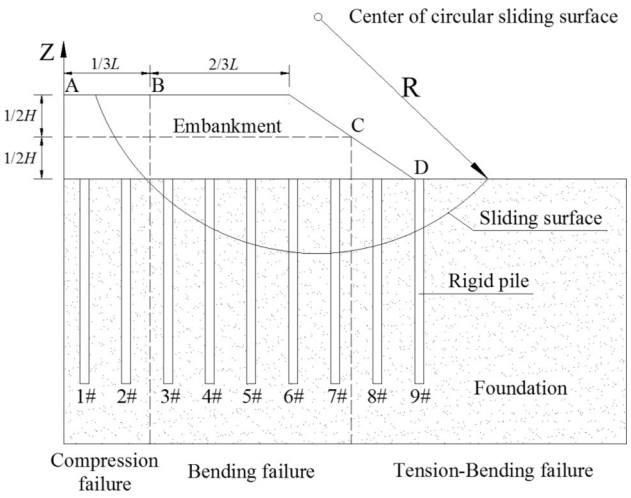

Fig. 17 Different failure modes of pile shaft at different regions

foundation under embankment, the compressive bearing capacity of piles under the center of embankment should be guaranteed, and the bending strength of piles under the shoulder of embankment should be large enough to avoid bending failure; for the piles under the slope toe of embankment, the bending strength and tensile strength of the pile shaft should be guaranteed to avoid bending failure or tensile failure. The PHC pile and plain concrete pile are mainly used in the rigid pile composite foundation, and the bending resistance and tensile resistance of these two piles are relatively small, and bending failure or tensile failure will probably occur. Hence, the reinforced concrete pile is recommended to be used under the shoulder and slope toe of the embankment.

The shear stress of the pile shaft under flexible foundation is not very large and the possibility of shearing failure of pile shaft is small (Yu et al. [42, 43]). The test results in this research also show that the assumption of shearing failure of pile shaft in composite foundation under embankment overestimates the stability of composite foundation under embankment. The different failure modes of the piles at different regions should be considered in the stability analysis of composite foundation under embankment, and the different stress characteristics of the piles at different regions should be considered to give a reliable analysis on the stability of embankment.

5 Conclusion

The behavior of rigid pile composite foundation under embankment was investigated based on a centrifuge model test. The shaft stress of piles at different regions, the soil pressure and the variation of pore water pressure in the test

process were analyzed, and the following conclusions can be gained based on the test results:

a. The soil displacements in rigid pile composite foundation under embankment were different at different regions: obvious vertical displacement occurred in the soil under the center of embankment and the horizontal displacement was very small; both vertical and horizontal displacement occurred in the soil under the shoulder of embankment; and obvious horizontal displacement occurred in the soil under the slope toe of embankment; moreover, ground heave occurred near the slope toe of embankment.
b. The lateral load on the pile under the center of embankment was relatively small, and the pile under the center of embankment was mainly to support the vertical load from the embankment; while for the piles under the shoulder of embankment, large horizontal displacement occurred in the loading process and the pile-soil stress ratio decreased as the applied pressure increases; the pile-soil stress ratio under the center of embankment was about 1.4 times the pile-soil stress ratio under the shoulder of embankment.
c. The soil displacement had a large influence on the behavior and failure mode of the rigid piles in composite foundation, and the failure modes of piles at different regions were different; the compressive failure would probably occur for the pile under the center of the embankment, and bending failure would probably occur for the pile under the shoulder of embankment, for the pile under the slope toe of embankment, the tension-bending failure would probably occur in the loading process. The different failure modes of the piles at different regions should be considered in the design of composite foundation under embankment, and the reinforced concrete pile was recommended to be used under the shoulder and slope toe of embankment;
d. The assumption of shearing failure of rigid pile shaft along the sliding surface overestimated the stability of the rigid pile composite foundation. The sliding resistances of the piles at different regions should be calculated separately to give a reliable analysis on the stability of embankment.

Acknowledgement This research is funded by the National Natural Science Foundation of China (Grant No. 51978610).

References

1. Blanc M, Rault G, Thorel L, Almeida MSS (2013) Centrifuge investigation of load transfer mechanisms in a granular mattress above a rigid inclusions network. Geotext Geomembr 36:92–105
2. Blanc M, Thorel L, Girout R, Almeida MSS (2014) Geosynthetic reinforcement of a granular load transfer platform above rigid inclusions: comparison between centrifuge testing and analytical modelling. Geosynth Int 21(1):37–52
3. Briançon L, Simon B (2010) Full-scale experiments of pile-supported earth platform under a concrete floor slab and an embankment. In: Invited speaker proceedings of symposium: new techniques for design and construction in soft clays, May 22–23 2010, Guaruja, Brazil
4. Briançon L, Simon B (2012) Performance of pile-supported embankment over soft soil: full-scale experiment. J Geotech Geoenviron Eng 138(4):551–561
5. Broms BB (2003) Deep soil stabilization: design and construction of lime and lime/cement columns. R Inst Technol, Stockholm
6. Chen RP, Chen YM, Han J, Xu ZZ (2008) A theoretical solution for pile-supported embankments on soft soils under one-dimensional compression. Can Geotech J 45:611–623
7. Chen RP, Wang YW, Ye XW, Bian XC, Dong XP (2016) Tensile force of geogrids embedded in pile-supported reinforced embankment: a full-scale experimental study. Geotext Geomembr 44(2):157–169
8. Diego F, Marcio SS, Luc T, Matthieu B (2017) Load transfer mechanism and deformation of reinforced piled embankments. Geotext Geomembr 45(2):1–10
9. Filz MG, Smith ME (2007) Net vertical loads on geosynthetic reinforcement in column-supported embankments. In: Proceedings of sessions of geo-denver 2007, soil improvement (GSP 172). ASCE, Denver, Colorado, USA, p 12
10. Gourvenec S, Acosta-Martinez HE, Randolph MF (2009) Experimental study of uplift resistance of shallow skirted foundations in clay under transient and sustained concentric loading. Géotechnique 59(6):525–537
11. Han J, Huang J, Porbaha A (2005) 2D Numerical modeling of a constructed geosynthetic-reinforced embankment over deep mixed columns. In: ASCE GSP 131, contemporary issues in foundation engineering, 2005
12. Hashizume H (1998) Study on the behavior of soft ground improved using deep mixing method. In: Proceedings of the international conference on centrifuge, vol 98, pp 851–856
13. Hewlett WJ, Randolph MF (1988) Analysis of piled embankments. Ground Eng 21(3):12–18
14. Huang J, Han J, Porbaha A (2006) Two and three-dimensional modeling of DM columns under embankments. ASCE Geo Congress
15. Jenck O, Dias D, Kastner R (2007) Two-dimensional physical and numerical modeling of a pile-supported earth platform over soft soil. J Geotech Geoenviron Eng 133(3):295–305
16. Jenck O, Dias D, Kastner R (2009) Three-dimensional numerical modeling of a piled embankment. Int J Geomech 9(3):102–112
17. Jenck O, Dias D, Kastner R (2009) Discrete element modelling of a granular platform supported by piles in soft soil—validation on a small scale model test and comparison to a numerical analysis in a continuum. Comput Geotech 36:917–927
18. JTG D30-2015 (2015) Specification for design of highway subgrades. Ministry of Transport of the People's Republic of China, 2015 (**in Chinese**)
19. Kempfert H-G, Göbel C, Alexiew D, Heitz C (2004) German recommendations for reinforced embankments on pile similar elements. In: 3rd European geosynthetic conference, DGGT (German Geotechnical Society), vol 1, pp 279–285
20. Kempton GT, Russell D, Pierpoint N, Jones CJPF (1998) Two and three dimensional numerical analysis of the performance of geosynthetics carrying embankment loads over piles. In: Proceedings of the 6th international conference on geosynthetics, Atlanta, Georgia

21. Kitazume M, Maruyama K (2005) Collapse failure of group column type deep mixing improved ground under embankment. In: Proceedings of the international conference on deep mixing, ASCE, 2005, pp 245–254
22. Kitazume M, Maruyama K (2006) External stability of group column type deep mixing improved ground under embankment loading. Soils Found 46(3):323–340
23. Kitazume M, Maruyama K (2007) Internal stability of group column type deep mixing improved ground under embankment loading. Soils Found 47(3):437–455
24. Kitazume M, Okano K, Miyajima S (2000) Centrifuge model tests on failure envelope of column type deep mixing method improved ground. Soils Found 40(4):43–55
25. Lai H, Zheng J, Cui M et al (2020) "Soil arching" for piled embankments: insights from stress redistribution behaviour of DEM modelling. Acta Geotech 15:2117–2136
26. Low BK, Tang SK, Choa V (1994) Arching in piled embankments. J Geotech Eng 120(11):1917–1937
27. Lv WZ, Yu JL, Liu C, Gong XN, Jing ZJ (2009) Load transfer rule of composite ground under flexible foundation. China J Highw Transp 32(5):657–663 **(in Chinese)**
28. Miyake M, Akamoto H, Wada M (1991) Deformation characteristics of ground improved by a group of treated soil. In: Centrifuge 91. Rotterdam: Balkema, pp 295–302
29. Naughton PJ (2007) The significance of critical height in the design of piled embankment. In: Proceedings of sessions of geo-denver 2007, soil improvement (GSP 172). Geo-institute, ASCE, Denver, Colorado, USA, p 12
30. Navin MP, Filz GM (2006) Numerical stability analyses of embankments supported on deep mixed columns. In: ASCE GSP 152, ground modification and seismic mitigation
31. Nunez M, Briançon L, Dias D (2013) Analyses of a pile-supported embankment over soft clay: full-scale experiment, analytical and numerical approaches. Eng Geol 153(8):53–67
32. Rowe RK, Liu KW (2015) Three-dimensional finite element modelling of a fullscale geosynthetic reinforced, pile-supported embankment. Can Geotech J 52(12):2041–2054
33. Russell D, Pierpoint N (1997) An assessment of design methods for piled embankments. Ground Eng 30(11):39–44
34. Terashi M, Tanaka H, Kitazume M (1983) Extrusion failure of the ground improved by the deep mixing method. In: Proceedings of the 7th Asian regional conference on soil mechanics and foundation engineering: Haifa, Israel, pp 313–318
35. The Deep Mixing Method-Principle, Design and Construction. Coastal Development Institute Tokyo, A.A. Balkema Publishers, 2002
36. Van Eekelen SJM, Bezuijen A, Lodder HJ, van Tol AF (2012) Model experiments on piled embankments. Part I. Geotext Geomembr 32:69–81
37. Van Eekelen SJM, Bezuijen A, Lodder HJ, Van Tol AF (2012) Model experiments on piled embankments, part II. Geotext Geomembr 32:82–94
38. Wachman G, Biolzi L, Labuz J (2010) Structural behavior of a pile-supported embankment. J Geotech Geoenviron Eng 136:26–34
39. Xing H, Zhang Z, Liu H, Wei H (2014) Large-scale tests of pile-supported earth platform with and without geogrid. Geotext Geomembr 42(6):586–598
40. Yu JL, Gong XN, Jiang P (2007) Working behavior of composite ground improved by rigid piles under flexible foundation. China J Highw Transp 20(4):1–6 **(in Chinese)**
41. Yu JL, Jing ZJ, Gong XN, Liu C, Lv WZ (2010) Working behaviors of composite ground under flexible foundation based on super-sub structure interaction. Chin J Geotech Eng 32(5):657–663 **(in Chinese)**
42. Yu JL, Li JY, Wang CW, Zhang JL, Gong XN, Chen CF, Song Er X (2017) Stability of composite foundation improved by rigid piles under embankment considering different failure modes of piles. Chin J Geotech Eng 39(S2):37–40 **(in Chinese)**
43. Yu JL, Wang CW, Xie YM, Zhang JL, Gong XN (2017) Analysis of stress and failure mechanism on composite foundation improved by rigid piles under flexible foundation considering damage of piles. J Central South Univ (Sci Technol) 48(9):2432–2440 **(in Chinese)**
44. Zeng KH, Yu JL, Gong. XN (2004) Analysis of performance of LSC pile composite ground under the load from embankment. J Zhejiang Univ (Eng Sci) 38(2):185–190 **(in Chinese)**
45. Zhang Z, Rao F, Ye G (2020) Design method for calculating settlement of stiffened deep mixed column-supported embankment over soft clay. Acta Geotech 15:795–814
46. Zheng G, Yang X, Zhou H, Chai J (2019) Numerical modeling of progressive failure of rigid piles under embankment load. Can Geotech J 56(1):23–34
47. Zhou H, Zheng G, Liu J et al (2019) Performance of embankments with rigid columns embedded in an inclined underlying stratum: centrifuge and numerical modelling. Acta Geotech 14:1571–1584